Effect of High-Temperature Annealing on the Elastoplastic Response of Isotactic Polypropylene in Loading–Unloading Tests

A. D. Drozdov, J. de C. Christiansen

Department of Production, Aalborg University, Fibigerstraede 16, DK-9220 Aalborg, Denmark

Received 8 June 2002; accepted 29 December 2002

ABSTRACT: A series of uniaxial tensile loading–unloading tests is performed on isotactic polypropylene at room temperature. Prior to mechanical testing, injection-molded specimens are annealed for 24 h at temperatures T = 145, 150, 155, 158, 160, 163, and 165°C, which cover the entire region of high-temperature annealing temperatures. A constitutive model is developed for the elastoplastic behavior of a semicrystalline polymer at small strains. The stress–strain relations are determined by six adjustable parameters that are found by matching observations in cyclic tests. Fair agreement is demonstrated between the experimental data and the results of numerical simulation. It is shown that all material constants are affected by the annealing temperature, which is explained by changes in the crystalline morphology driven by thermal treatment. Some of the adjustable parameters experience finite jumps in the vicinity of the critical temperature T_c = 159°C. These jumps are attributed to the $\alpha_2 \rightarrow \alpha_2'$ phase transformation. © 2003 Wiley Periodicals, Inc. J Appl Polym Sci 90: 186–196, 2003

Key words: annealing; poly(propylene); structure–property relations; tensions

INTRODUCTION

This article is concerned with the effect of high-temperature annealing (in the region of temperatures between 140 and 166°C) on the elastoplastic response of injection-molded isotactic polypropylene (iPP) in isothermal uniaxial cyclic tests with small strains. The elastoplastic and viscoplastic behavior of iPP has been the focus of attention in the past decade, which may be explained by numerous industrial applications of this polymer (ranging from oriented films for packaging to nonwoven fabrics and reinforcing fibers).

Annealing and isothermal crystallization of iPP have attracted substantial attention in the past 5 years.[1–8] This interest may be attributed to noticeable changes in the crystalline morphology driven by thermal treatment.

iPP is a semicrystalline polymer containing three basic crystallographic forms[5]: monoclinic α crystallites, (pseudo)hexagonal β structures, orthorhombic γ polymorphs, and "smectic" mesophase (arrays of chains with a better order in the longitudinal than in the transverse chain direction). At rapid cooling of the melt (which is typical of the injection-molding process), α crystallites and smectic mesophase are developed mainly, whereas β and γ polymorphs are observed as minor components.[9]

The characteristic size of α spherulites in an injection-molded specimen is estimated as 100–200 μm.[9,10] These spherulites consist of lamellae with thicknesses ranging from 10 to 20 nm.[6,10] A unique feature of α polymorphs in iPP is lamellar cross-hatching: development of transverse lamellae oriented in the direction perpendicular to the direction of radial lamellae in spherulites.[5,6]

The α structures in iPP are characterized by a monoclinic unit cell containing four chains in a helical conformation.[11] Due to the presence of asymmetrically substituted methyl groups, the helices acquire "up" and "down" orientations. This implies that some cells contain only ordered helices (whose directions coincide), whereas other cells are characterized by some level of disorder (in these cells, chains with opposite directions are packed). Following ref. 12, two limiting modifications are conventionally analyzed: (i) a statistically disordered α_1 phase and (ii) an ordered α_2 phase that is characterized by a regular distribution of helices with up and down orientations.

Transmission electron microscopy (TEM)[2,6] and polarized optical microscopy[2] show that the growth of annealing temperature results in (i) a decrease in the concentration of transverse lamellae and the total disappearance of cross-hatching at annealing above 150°C and (ii) an increase in the fraction of α_2 crystallites; their fraction reaches unity at the annealing tem-

Correspondence to: A. D. Drozdov, Department of Chemical Engineering, West Virginia University, P.O. Box 6102, Morgantown, WV 26506 (Aleksey.Drozdov@mail.wvu.edu).

Journal of Applied Polymer Science, Vol. 90, 186–196 (2003)

perature of 150°C, but it can decrease at higher temperatures.[13]

Recent wide-angle X-ray diffraction (WAXD) measurements[6,8] revealed that the annealing of iPP in the vicinity of the critical temperature $T_c = 159$°C induces a second-order phase transition in which the α_2 crystallographic form is replaced by a new α_2' form with a higher lattice spacing. It was suggested[8] that the mobility of chains in the new phase noticeably exceeds that in the α_2 phase, because the chains are loosely packed. This increase in mobility of macromolecules is confirmed by TEM observations, which show a pronounced increase in the maximum lamellar thickness.[8] The latter is attributed to the fact that the growth of a lattice spacing promotes the "sliding diffusion" of chains, which is thought of as a mechanism for lamellar thickening.

It is natural to assume that the $\alpha_2 \rightarrow \alpha_2'$ transformation induces pronounced changes in the elastoplastic and viscoplastic behavior of iPP, because the mobility of chains plays the key role in the nonlinear response of polymers. However, to the best of our knowledge, appropriate experiments have not yet been performed.

The objective of the present study was threefold:

1. To report experimental data in uniaxial tensile loading–unloading tests on iPP annealed at several temperatures in the vicinity of the critical temperature T_c.
2. To develop constitutive equations for the elastoplastic behavior of a semicrystalline polymer and to determine adjustable parameters in the stress–strain relations by fitting the observations.
3. To assess the effect of the annealing temperature, T, on the experimental constants and to demonstrate that some of them undergo finite jumps at T_c.

Injection-molded isotactic propylene is treated as a composite medium consisting of developed α spherulites, nonperfect lamellar stacks, smectic mesophase, and two amorphous phases: (i) mobile (located between spherulites and in "liquid pockets"[14] between lamellar stacks) and (ii) constrained (the so-called "rigid amorphous fraction"[14] located between radial and tangential lamellae in lamellar stacks). Stretching of iPP specimens induces two types of structural transformations. At the microlevel, one observes (i) nucleation and propagation of dislocations in crystallites (driven by a twist of stems and changes in the step length in helices[15]), (ii) chain slip through the crystals, and (iii) sliding and separation of tie chains.[16,17] At the mesolevel, these transformations are revealed as (i) interlamellar separation, (ii) rotation and twist of lamellae, (iii) fine and coarse slip of lamellar blocks and their fragmentation,[18] and (iv) activation of rigid amorphous fraction induced by lamellae disintegration.

To describe these changes in the microstructure of iPP within a constitutive model with a small number of adjustable parameters, we apply a method of homogenization of the microstructure.[19] According to this approach, a semicrystalline polymer is treated as an equivalent network of chains bridged by junctions (entanglements, physical crosslinks, and lamellar blocks). Our choice of an amorphous phase as an equivalent phase is grounded on the following reasons:

1. The time-dependent response of iPP is traditionally associated with rearrangement of chains in amorphous regions.[10]
2. Plastic flow in semicrystalline polymers is assumed to be "initiated in the amorphous phase before transitioning into the crystalline phase."[20]
3. Conventional models for the viscoplastic behavior of PP treat it as a network of macromolecules.[21,22]

The equivalent network is assumed to be strongly heterogeneous, and it is thought of as an ensemble of mesoregions (MRs). The heterogeneity of the network is attributed to an inhomogeneity of interactions between chains in the amorphous phase and crystalline lamellae with various lengths and thicknesses.

An MR is treated as a network of chains bridged by junctions. The mechanical response of an MR is attributed to that of the amorphous phase, whereas the links between mesodomains (that transmit the macrostrain to individual MRs) reflect the response of crystallites.

A mesoregion is modeled as a linear elastic medium. Deviations of the stress–strain curves in tensile tests from straight lines (that correspond to the response of a linear elastic solid) are ascribed to sliding of junctions between chains with respect to their reference positions. Elastic deformation of spherulites, interlamellar separation, and fine slip of lamellar blocks are not included in the model explicitly, but are taken into account implicitly in terms of "average" parameters that characterize sliding of junctions in mesodomains. This "generalized" sliding process is described by a plastic strain, ϵ_{p1}, whose rate of growth is proportional to the rate of the macrostrain.

At retraction, junctions between chains in MRs move back to their initial positions driven by a decrease in the macrostrain ϵ. To account for the microfracture of crystallites (observed as coarse slip and disintegration of lamellar blocks at unloading), another plastic strain, ϵ_{p2}, is introduced, which increases in time with a rate proportional to the elastic strain.

It is worth noting a similarity between splitting of the plastic strain, ϵ_p, into two components, ϵ_{p1} and ϵ_{p2},

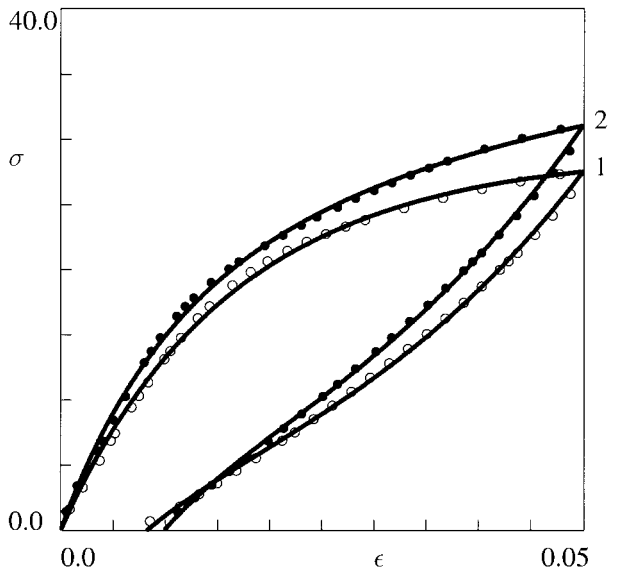

Figure 1 Stress σ (MPa) versus strain ϵ in tensile loading–unloading tests. (Symbols) Experimental data. (Unfilled circles) A nonannealed specimen; (filled circles) a specimen annealed at $T = 145°C$. (Solid lines) Results of numerical simulation.

where the latter quantity is altered at unloading only, and the Ogden–Roxburgh model[23] for the Mullins effect in particle-reinforced elastomers. According to ref. 23, the difference between the stress–strain curves at active deformation and unloading is attributed to some damage parameter that changes at retraction only. An advantage of our approach compared to the previous one is that the plastic strain, ϵ_{p2}, obeys a conventional flow rule in elastoplasticity, whereas the damage parameter introduced in ref. 23 is governed by a kinetic equation whose physical meaning is not transparent for semicrystalline polymers.

EXPERIMENTAL

iPP (Novolen 1100L) was supplied by BASF (Targor Gmbh, Mainz, Germany). ASTM dumbbell specimens, with length of 148 mm, width of 9.8 mm, and thickness of 3.8 mm, were injection-molded. Uniaxial tensile tests were performed at room temperature on a testing machine Instron-5568 equipped with electromechanical sensors for the control of longitudinal strains in the active zone of the samples. The tensile force was measured by a standard load cell. The longitudinal stress, σ, was determined as the ratio of the axial force to the cross-sectional area of stress-free specimens.

The series of experiments consists of eight tests on a specimen not subjected to thermal treatment and on samples annealed for 24 h at the temperatures $T = 145$, 150, 155, 158, 160, 163, and 165°C and slowly cooled by air. To minimize the effect of physical aging, mechanical tests were carried out at least 1 day after the thermal treatment.

In each test, a specimen was stretched with a crosshead speed of 10 mm/min (which corresponds to the strain rate $\dot{\epsilon}_0 = 2.09 \times 10^{-4}\ s^{-1}$) up to the maximal strain, $\epsilon_{max} = 0.05$, and unloaded with the same crosshead speed down to zero stress. The chosen crosshead speed ensures nearly isothermal experimental conditions,[24] on the one hand, and it is sufficiently large to disregard the viscoelastic effects, on the other (the maximal duration of a cyclic test does not exceed 1 min).

The experimental data are presented in Figures 1–4, where the engineering stress, σ, is plotted versus the engineering strain, ϵ. The stress–strain diagrams for nonannealed specimens, as well as for samples annealed at various temperatures in the interval from 145 to 165°C, have similar shapes. The following features of these curves are worthy to be mentioned:

1. The loading and unloading paths of the stress–strain curves substantially differ from each other.
2. The unloading curves are strongly nonlinear.
3. Given a strain, ϵ, the stress, σ, monotonically increases with the annealing temperature (which may be associated with an increase in the degree of crystallinity).
4. The residual strain (measured at the instant when the stress vanishes) is weakly affected by the thermal treatment.

According to Figures 1–4, the shape of the stress–strain curves does not change substantially with the

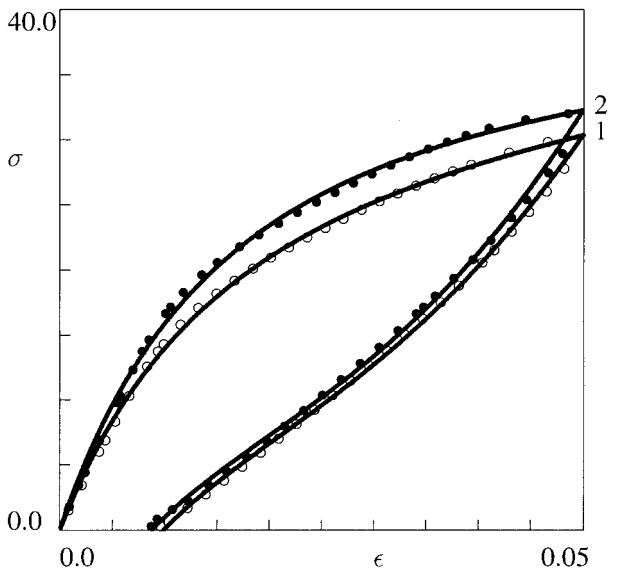

Figure 2 Stress σ (MPa) versus strain ϵ in tensile loading–unloading tests. (Symbols) Experimental data. (Unfilled circles) A specimen annealed at $T = 150°C$; (filled circles) a specimen annealed at $T = 155°C$. (Solid lines) Results of numerical simulation.

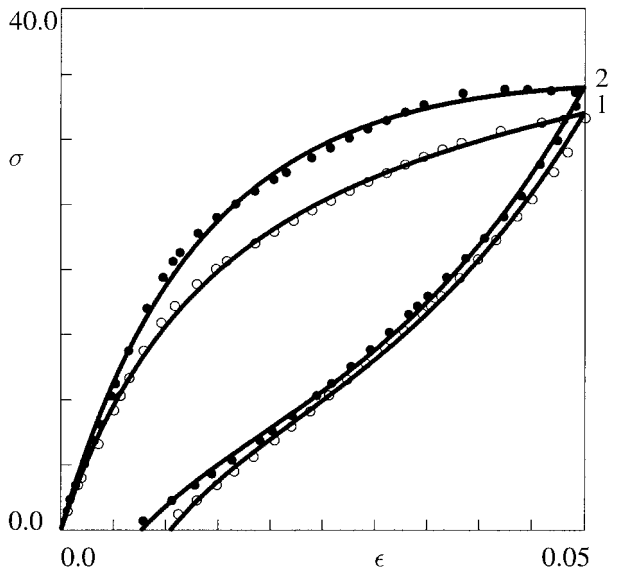

Figure 3 Stress σ (MPa) versus strain ϵ in tensile loading–unloading tests. (Symbols) Experimental data. (Unfilled circles) A specimen annealed at $T = 158$°C; (filled circles) a specimen annealed at $T = 160$°C. (Solid lines) Results of numerical simulation.

annealing temperature in the entire interval of temperatures under consideration, including the close vicinity of the critical temperature, T_c. This conclusion is, however, grounded on the qualitative study of the stress–strain diagrams. Our purpose is to derive a constitutive model for the elastoplastic behavior of a semicrystalline polymer and to demonstrate (based on the quantitative analysis) that some adjustable parameters in the stress–strain relations experience finite jumps at T_c.

MICROMECHANICAL MODEL

A semicrystalline polymer is treated as a strongly heterogeneous network of chains. The network is modeled as an ensemble of mesoregions with arbitrary shapes and sizes. The characteristic length of an MR substantially exceeds the radius of gyration for a macromolecule, and it is noticeably less than the size of a sample.

Deformation of a specimen induces two processes in the network.

1. Sliding of junctions (physical crosslinks and entanglements that bridge chains in the network) with respect to their reference positions in a stress-free medium.
2. Sliding of mesodomains in the ensemble with respect to each other.

Sliding of junctions describes nonaffine deformation of a network. This process is determined by a plastic strain ϵ_{p1}. Sliding of MRs with respect to each other is characterized by a plastic strain ϵ_{p2}. In a semicrystalline polymer, the strain, ϵ_{p1}, reflects sliding of junctions in the amorphous phase, slippage of tie chains, and fine slip of lamellar blocks. The strain, ϵ_{p2}, describes coarse slip and disintegration of lamellar blocks.

The total plastic strain, ϵ_p, equals the sum of the plastic strains driven by sliding of junctions and mutual displacement of mesodomains:

$$\epsilon_p = \epsilon_{p1} + \epsilon_{p2} \tag{1}$$

Mesoregions that form a network are connected one with another by links that transmit the macrostrain, ϵ, to individual MRs. This implies the conventional hypothesis that the macrostrain, ϵ, equals the sum of the elastic strain in MRs, ϵ_e, and the plastic strain, ϵ_p:

$$\epsilon = \epsilon_e + \epsilon_p \tag{2}$$

To simplify the analysis, we assume that the elastic strains in various MRs coincide.

Deformation of a specimen results in evolution of the plastic strain, ϵ_{p1}, both at the stages of active loading and unloading. It is assumed that the rate of changes in the plastic strain, ϵ_{p1}, is proportional to the rate of changes in the macrostrain, ϵ:

$$\frac{d\epsilon_{p1}}{dt}(t) = \varphi[\epsilon_e(t)]\,\frac{d\epsilon}{dt}(t) \tag{3}$$

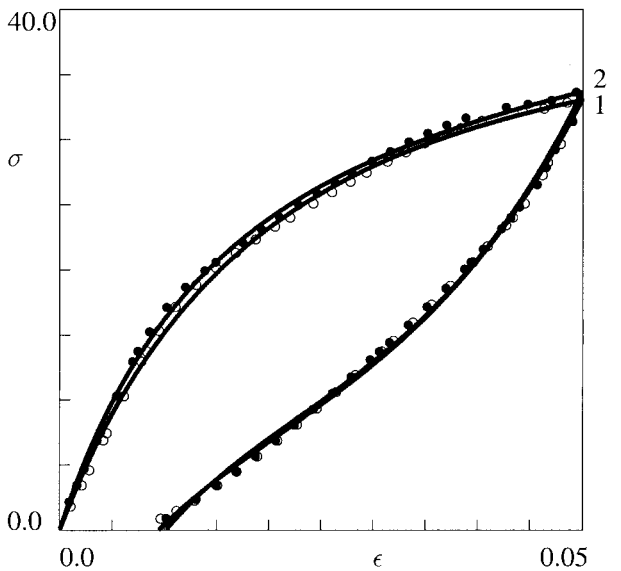

Figure 4 Stress σ (MPa) versus strain ϵ in tensile loading–unloading tests. (Symbols) Experimental data. (Unfilled circles) A specimen annealed at $T = 163$°C; (filled circles) a specimen annealed at $T = 165$°C. (Solid lines) Results of numerical simulation.

where the coefficient of proportionality, φ, depends on the elastic strain ϵ_e. The function $\varphi(\epsilon_e)$ vanishes at zero elastic strain, $\varphi(0) = 0$, monotonically increases with ϵ_e, and tends to some constant $a \in [0, 1]$ at relatively large elastic strains:

$$\lim_{\epsilon_e \to \infty} \varphi(\epsilon_e) = a$$

where a is the rate of sliding of junctions for a developed plastic flow. The inequality $a \geq 0$ means that junctions slide in the direction that is determined by the macrostrain ϵ. The condition $a \leq 1$ ensures that the rate of sliding does not exceed the rate of the macrostrain.

To approximate the experimental data, we employed the phenomenological relation

$$\varphi(\epsilon_e) = a\left[1 - \exp\left(-\frac{\epsilon_e}{\varepsilon}\right)\right] \tag{4}$$

This function is determined by two adjustable parameters, a and ε, where the strain, ε, characterizes the transition to a steady plastic flow.

Separation of tie chains from lamellae and disintegration of lamellar blocks result in a decrease in the number of MRs to which the macrostrain, ϵ, is transmitted by surrounding mesodomains. This decrease reflects (i) mechanically induced separation of individual MRs from the ensemble and (ii) screening of mesodomains by stacks of disintegrated lamellae.

To describe evolution of an ensemble of mesodomains, we introduce the average number of MRs, N_0, per unit mass of a virgin specimen (where all MRs are connected to one another) and the average number of MRs, $N(t)$, in the deformed specimen at time $t \geq 0$ (where some mesoregions are separated from the ensemble). Following refs. 15 and 18, we suppose that, at active loading in the subyield region of deformations, lamellar fragmentation does not occur, which implies that separation of MRs does not take place and the number of MRs in the ensemble, $N(t)$, remains constant:

$$\frac{dN}{dt}(t) = 0 \qquad \left[\frac{d\epsilon}{dt}(t) \geq 0, \qquad \sigma(t) \geq 0\right], \qquad N(0) = N_0 \tag{5}$$

At retraction, the function $N(t)$ monotonically decreases. This decrease is attributed to fragmentation of lamellar blocks and formation of disordered lamellar stacks. These stacks do not transmit the macrostrain, ϵ, to the amorphous domains surrounded by them, which results in isolation of these regions from the ensemble (in a way similar to formation of regions of occluded rubber in a particle-reinforced elastomer[25]).

Changes in the function $N(t)$ at unloading are governed by a first-order kinetic equation, according to which the relative number of MRs separated from the ensemble per unit time is proportional to the increment of the plastic strain, ϵ_{p2}, which reflects disintegration of lamellar blocks:

$$-\frac{1}{N(t)}\frac{dN}{dt}(t) = \frac{1}{\varepsilon_1}\frac{d\epsilon_{p2}}{dt}(t) \qquad \left[\frac{d\epsilon}{dt}(t) < 0, \qquad \sigma(t) \geq 0\right] \tag{6}$$

where the strain ε_1 characterizes the influence of lamellar fragmentation on the separation of MRs from the ensemble.

As lamellar fragmentation does not occur at active loading in the subyield region of deformations, the plastic strain, ϵ_{p2}, vanishes:

$$\frac{d\epsilon_{p2}}{dt}(t) = 0 \qquad \left[\frac{d\epsilon}{dt}(t) \geq 0, \qquad \sigma(t) \geq 0\right] \tag{7}$$

which means that, at active deformation, displacements of MRs with respect to each other are disregarded.

At retraction, mesodomains slide with respect to each other as they are driven by a positive macrostress σ. These mutual displacements of MRs are characterized by a plastic strain, ϵ_{p2}, that grows with time. An increase in ϵ_{p2} at unloading reflects coarse slip and fragmentation of deformed lamellae. The evolution of the plastic strain, ϵ_{p2}, is described by the flow rule:

$$\frac{d\epsilon_{p2}}{dt}(t) = \Gamma[\epsilon_e(t)]\epsilon_e(t) \qquad \left[\frac{d\epsilon}{dt}(t) < 0, \qquad \sigma(t) \geq 0\right] \tag{8}$$

Equation (8) means that the rate of changes in ϵ_{p2} is proportional to the elastic strain, ϵ_e. By analogy with eq. (3), the coefficient of proportionality, Γ, is thought of as a function of the elastic strain. It is assumed that the process of lamellar fragmentation at retraction has an avalanchelike character (which means that the number of fragmentation events per unit time grows with the number of disintegrated lamellar blocks). Such a dependence can be captured by a phenomenological equation

$$\Gamma(\epsilon_e) = \Gamma_0 \exp\left(-\frac{\epsilon_e}{\varepsilon_2}\right) \tag{9}$$

where the prefactor, Γ_0, determines the rate of plastic strain, ϵ_{p2}, at small elastic strains and the quantity ε_2 characterizes a decrease in the rate of the plastic strain, Γ, with the elastic strain. It is worth noting that eqs. (8)

and (9) are proposed to describe changes in the plastic strain, ϵ_{p2}, at unloading, when the parameter Γ increases from its initial value (corresponding to the maximal macrostrain, ϵ_{max}) to Γ_0 (which is reached at the end of the unloading path, when the stress, σ, vanishes).

CONSTITUTIVE EQUATIONS

Under isothermal uniaxial deformation, a mesodomain is treated as a linear elastic solid with the mechanical energy:

$$w = \frac{1}{2}\,\mu\epsilon_e^2$$

where the constant $\mu > 0$ is the average rigidity of an MR. Neglecting the energy of interaction between mesoregions, we calculate the strain energy density per unit mass of a polymer as the sum of the mechanical energies of MRs:

$$W(t) = \frac{\mu}{2}\,N(t)\epsilon_e^2 \tag{10}$$

It follows from eqs. (1)–(3) and (10) that the derivative of the function W with respect to time is given by

$$\frac{dW}{dt}(t) = \frac{\mu}{2}\frac{dN}{dt}(t)\epsilon_e^2(t) + \mu N(t)\epsilon_e(t)\left(\{1 - \varphi[\epsilon_e(t)]\}\frac{d\epsilon}{dt}(t) - \frac{d\epsilon_{p2}}{dt}(t)\right) \tag{11}$$

The Clausius–Duhem inequality reads

$$Q(t) = -\frac{dW}{dt}(t) + \frac{1}{\rho}\,\sigma(t)\frac{d\epsilon}{dt}(t) \geq 0$$

where ρ is the mass density, and Q, the internal dissipation per unit mass. Substitution of eq. (11) into this formula results in

$$Q(t) = \frac{1}{\rho}\left(\sigma(t) - \rho\mu N(t)\epsilon_e(t)\{1 - \varphi[\epsilon_e(t)]\}\right)\frac{d\epsilon}{dt}(t) + Y(t) \geq 0 \tag{12}$$

where

$$Y(t) = \mu N(t)\epsilon_e(t)\left[\frac{d\epsilon_{p2}}{dt}(t) - \frac{1}{2N(t)}\frac{dN}{dt}(t)\epsilon_e(t)\right] \tag{13}$$

Equating the expression in parentheses in eq. (12) to zero, we arrive at the constitutive equation

$$\sigma(t) = E(t)\epsilon_e(t)\{1 - \varphi[\epsilon_e(t)]\} \tag{14}$$

where

$$E(t) = \rho\mu N(t) \tag{15}$$

Equations (5), (7), and (13) imply that

$$Y(t) = 0 \qquad \left[\frac{d\epsilon}{dt}(t) \geq 0, \qquad \sigma(t) \geq 0\right] \tag{16}$$

It follows from eqs. (6), (8), and (13) that

$$Y(t) = \mu N(t)\left[1 + \frac{\epsilon_e(t)}{2\varepsilon_1}\right]\Gamma[\epsilon_e(t)]\epsilon_e^2(t) \qquad \left[\frac{d\epsilon}{dt}(t) < 0, \qquad \sigma(t) \geq 0\right] \tag{17}$$

Combining eqs. (12) and (14), we find that the internal dissipation per unit mass, $Q(t)$, coincides with $Y(t)$. According to eqs. (16) and (17), the function $Y(t)$ is nonnegative, which means that the Clausius–Duhem inequality is satisfied for an arbitrary deformation program, provided that the stress, σ, is given by eq. (14).

It follows from eqs. (5), (6), and (15) that the elastic modulus, E, obeys the differential equations

$$\frac{dE}{dt}(t) = 0, \qquad E(0) = E_0 \qquad \left[\frac{d\epsilon}{dt}(t) \geq 0, \qquad \sigma(t) \geq 0\right]$$
$$\frac{1}{E(t)}\frac{dE}{dt}(t) = -\frac{1}{\varepsilon_1}\frac{d\epsilon_{p2}}{dt}(t) \qquad \left[\frac{d\epsilon}{dt}(t) < 0, \qquad \sigma(t) \geq 0\right] \tag{18}$$

where $E_0 = \mu\rho N_0$ is the elastic modulus of a virgin specimen.

Uniaxial deformation of a semicrystalline polymer is described by eqs. (1)–(4), (7)–(9), (14), and (18). Any stress–strain curve for cyclic loading is determined by six adjustable parameters: (i) the initial elastic modulus E_0, (ii) the rate, a, of the developed plastic flow, (iii) the strain, ε, which characterizes the transition to a steady plastic flow, (iv) the strain, ε_1, which characterizes separation of mesodomains from an ensemble, (v) the rate, Γ_0, of sliding of MRs with respect to each other, and (vi) the strain, ε_2, which characterizes mechanically induced changes in the rate of sliding.

This number of material constants is quite comparable with those in other constitutive relations in elastoplasticity of solid polymers.[26–30] It should be noted, however, that the previous models describe the response of solid polymers in cyclic tests rather poorly.[19] An advantage of the stress–strain relations (1)–(4), (7)–(9), (14), and (18) is that three constants, E_0, a, and

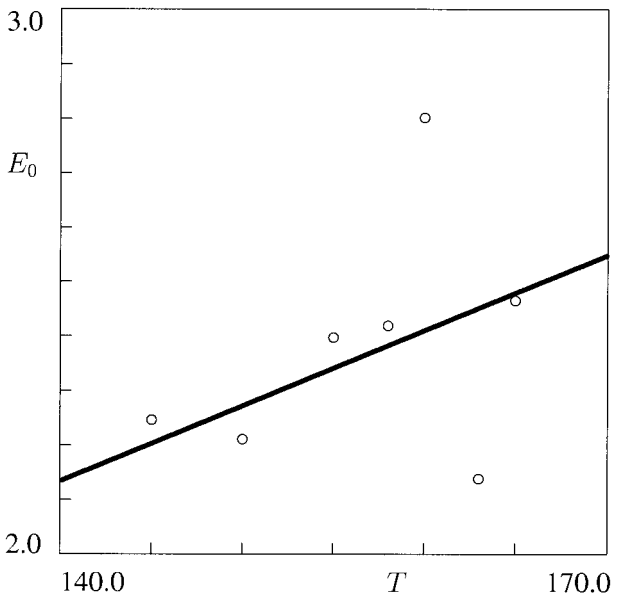

Figure 5 Elastic modulus E_0 (GPa) versus the annealing temperature T (°C). (Circles) Treatment of observations. (Solid lines) Approximation of the experimental data by eq. (21) with $c_0 = 0.20$ and $c_1 = 1.38 \times 10^{-2}$.

ε, are found by fitting the experimental data for the loading path of a stress–strain curve, whereas the other three parameters, Γ_0, ε_1, and ε_2, are determined by matching observations for the unloading path.

FITTING OF OBSERVATIONS

We begin with the approximation of the stress–strain diagrams for active loading. It follows from eqs. (1)–(4), (7), (14), and (18) that the stress, σ, is given by

$$\sigma(\epsilon) = E_0(\epsilon - \epsilon_{p1})\left\{1 - a\left[1 - \exp\left(-\frac{\epsilon - \epsilon_{p1}}{\varepsilon}\right)\right]\right\} \quad (19)$$

where the plastic strain, ϵ_{p1}, satisfies the nonlinear differential equation

$$\frac{d\epsilon_{p1}}{d\epsilon}(\epsilon) = a\left[1 - \exp\left(-\frac{\epsilon - \epsilon_{p1}}{\varepsilon}\right)\right], \qquad \epsilon_{p1}(0) = 0 \quad (20)$$

The loading path of any stress–strain curve is determined by three material constants: E_0, a, and ε. To find these quantities, we fix some intervals $[0, a_{\max}]$ and $[0, \varepsilon_{\max}]$, where the "best-fit" parameters a and ε are assumed to be located, and divide these intervals into J subintervals by the points $a^{(i)} = i\Delta a$ and $\varepsilon^{(j)} = j\Delta\varepsilon$ ($i, j = 1, \ldots, J - 1$), with $\Delta a = a_{\max}/J$ and $\Delta\varepsilon = \varepsilon_{\max}/J$. For any pair, $\{a^{(i)}, \varepsilon^{(j)}\}$, eq. (20) is integrated numerically by the Runge–Kutta method with the step $\Delta\epsilon = 1.0 \times 10^{-5}$. Given a pair, $\{a^{(i)}, \epsilon^{(j)}\}$, the elastic modulus, $E_0 = E_0(i, j)$, is found by the least-squares method from the condition of minimum of the function

$$F = \sum_{\epsilon_m} [\sigma_{\exp}(\epsilon_m) - \sigma_{\text{num}}(\epsilon_m)]^2$$

where the sum is calculated over all experimental points, ϵ_m, on a loading path, $\sigma_{\exp}$ is the stress measured in a tensile test, and σ_{num} is given by eq. (19). The "best-fit" parameters a and ε are determined from the condition of the minimum of the function F on the set $\{a^{(i)}, \varepsilon^{(j)}\ (i, j = 1, \ldots, J - 1)\}$.

The material constants, E_0, a, and ε, which minimize the discrepancies between the experimental data and the results of numerical analysis, are found for any stress–strain curve independently. These parameters are plotted versus the annealing temperature, T, in Figures 5–7. The experimental data are approximated by the linear functions

$$a = a_0 + a_1T, \qquad \varepsilon = b_0 - b_1T, \qquad E_0 = c_0 + c_1T \quad (21)$$

where the coefficients a_k, b_k, and c_k ($k = 0, 1$) are found by the least-squares technique. Figure 5 shows a rather good quality of matching the observations by eq. (21) (despite some scatter of the experimental data). According to Figures 6 and 7, eq. (21) provides an acceptable approximation of the observations with different coefficients, a_k and b_k, below and above the critical temperature, T_c.

To find the quantities, Γ_0, ε_1, and ε_2, we approximate the unloading paths of the stress–strain curves. It follows from eqs. (1)–(4), (8), (9), (14), and (18) that the stress, σ, is given by

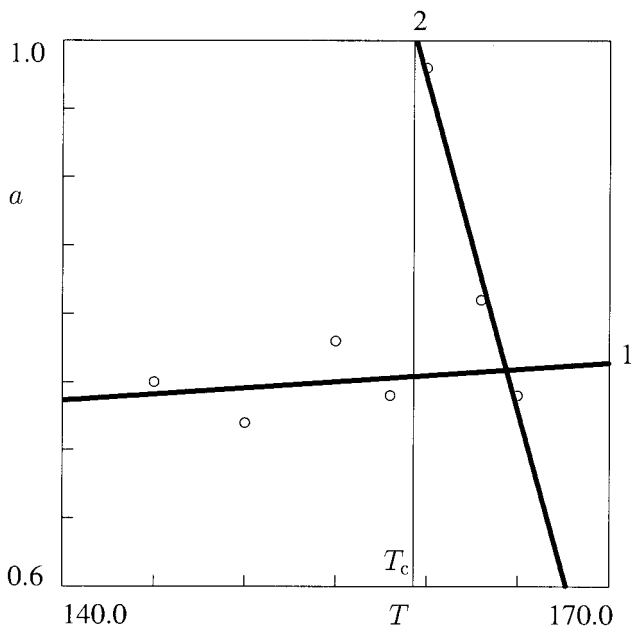

Figure 6 Rate of developed plastic flow a versus the annealing temperature T (°C). (Circles) Treatment of observations. (Solid lines) Approximation of the experimental data by eq. (21). (Curve 1) $a_0 = 0.61$; $a_1 = 9.18 \times 10^{-4}$; (curve 2) $a_0 = 8.76$; $a_1 = -4.87 \times 10^{-2}$.

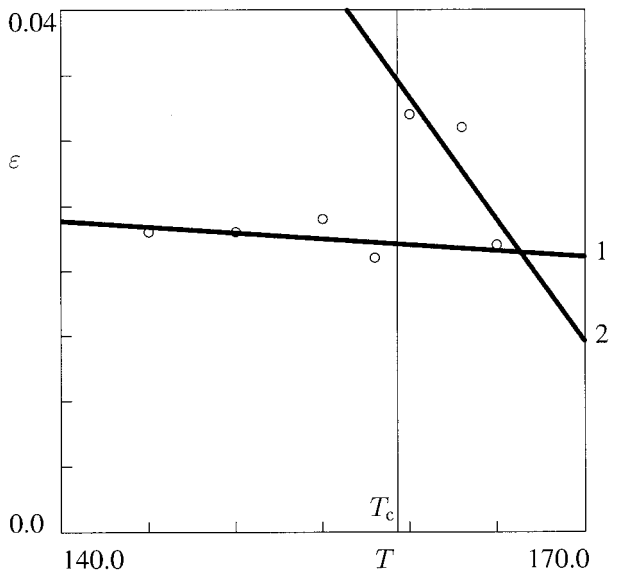

Figure 7 Strain ε for transition to a developed plastic flow versus the annealing temperature T (°C). (Circles) Treatment of observations. (Solid lines) Approximation of the experimental data by eq. (21). (Curve 1) $b_0 = 3.67 \times 10^{-2}$; $b_1 = 9.18 \times 10^{-5}$; (curve 2) $b_0 = 3.32 \times 10^{-1}$; $b_1 = 1.87 \times 10^{-3}$.

$$\sigma(\epsilon) = E(\epsilon_{p2})(\epsilon - \epsilon_{p1} - \epsilon_{p2}) \times \left\{1 - a\left[1 - \exp\left(-\frac{\epsilon - \epsilon_{p1} - \epsilon_{p2}}{\varepsilon}\right)\right]\right\} \quad (22)$$

where the elastic modulus, E, is

$$E(\epsilon_{p2}) = E_0 \exp\left(-\frac{\epsilon_{p2}}{\varepsilon_1}\right) \quad (23)$$

The plastic strains, ϵ_{p1} and ϵ_{p2}, obey the differential equations

$$\frac{d\epsilon_{p1}}{d\epsilon}(\epsilon) = a\left[1 - \exp\left(-\frac{\epsilon - \epsilon_{p1} - \epsilon_{p2}}{\varepsilon}\right)\right]$$

$$\frac{d\epsilon_{p2}}{d\epsilon}(\epsilon) = -\gamma(\epsilon - \epsilon_{p1} - \epsilon_{p2})\exp\left(-\frac{\epsilon - \epsilon_{p1} - \epsilon_{p2}}{\varepsilon_2}\right) \quad (24)$$

where

$$\gamma = \frac{\Gamma_0}{\dot{\epsilon}_0} \quad (25)$$

and $\dot{\epsilon}_0$ is the rate of the macrostrain. The "initial" conditions for eq. (24) are

$$\epsilon_{p1}(\epsilon_{max}) = \epsilon^0_{p1}, \qquad \epsilon_{p2}(\epsilon_{max}) = 0$$

where ϵ^0_{p1} is the maximal plastic strain, ϵ_{p1}, reached at active loading.

To approximate the experimental data at retraction, we apply an algorithm similar to that used to match the stress–strain curves at active loading. We fix some intervals $[0, \gamma_{max}]$, $[0, \varepsilon_{1\,max}]$, and $[0, \varepsilon_{2\,max}]$, where the "best-fit" parameters, γ, ε_1, and ε_2, are assumed to be located, and divide these intervals into J subintervals by the points $\gamma^{(i)} = i\Delta\gamma$, $\varepsilon_1^{(j)} = j\Delta\varepsilon_1$, and $\varepsilon_2^{(k)} = k\Delta\varepsilon_2$ (i, j, $k = 1, \ldots, J - 1$) with $\Delta\gamma = \gamma_{max}/J$, $\Delta\varepsilon_1 = \varepsilon_{1\,max}/J$, and $\Delta\varepsilon_2 = \varepsilon_{2\,max}/J$. Given a triple, $\{\gamma^{(i)}, \varepsilon_1^{(j)}, \varepsilon_2^{(k)}\}$, eqs. (22) to (24) are integrated numerically by the Runge–Kutta method with the step $\Delta\epsilon = 1.0 \times 10^{-5}$. For any set of experimental data, we use the parameters, E_0, a, and ε, found by fitting the loading path of an appropriate stress–strain curve. The maximal plastic strain, ϵ^0_{p1}, is determined by numerical integration of eq. (20) from $\epsilon = 0$ to $\epsilon = \epsilon_{max}$. The "best-fit" parameters, γ, ε_1, and ε_2, are found from the condition of the minimum of the function F on the set $\{\gamma^{(i)}, \varepsilon_1^{(j)}, \varepsilon_2^{(k)}$ ($i, j, k = 1, \ldots, J - 1$)$\}$.

Figures 1–4 demonstrate fair agreement between the experimental data and the results of numerical simulation. The dimensionless rate of plastic strain, γ, is plotted versus the annealing temperature, T, in Figure 8. The observations are approximated by the linear equation

$$\gamma = \gamma_0 + \gamma_1 T \quad (26)$$

where the coefficients γ_k ($k = 0, 1$) are found by the least-squares algorithm. Figure 8 shows an acceptable quality of fitting the experimental data by eq. (26) with

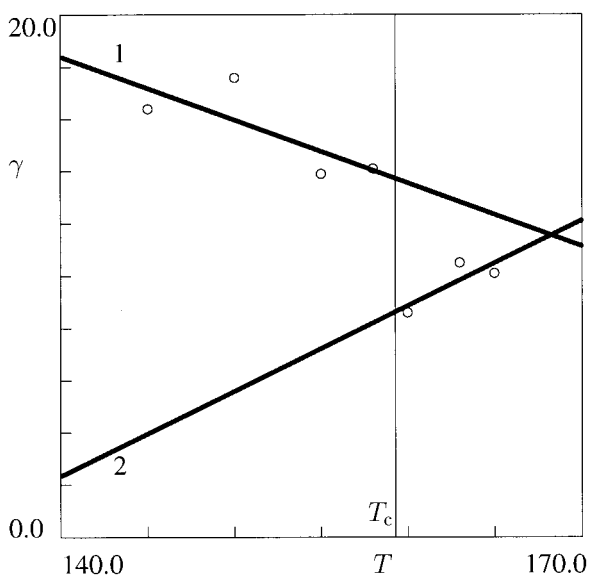

Figure 8 Rate of plastic strain at retraction γ_0 versus the annealing temperature T (°C). (Circles) Treatment of observations. (Solid lines) Approximation of the experimental data by eq. (26). (Curve 1) $\gamma_0 = 52.26$; $\gamma_1 = -0.24$; (curve 2) $\gamma_0 = -43.35$; $\gamma_1 = 0.33$.

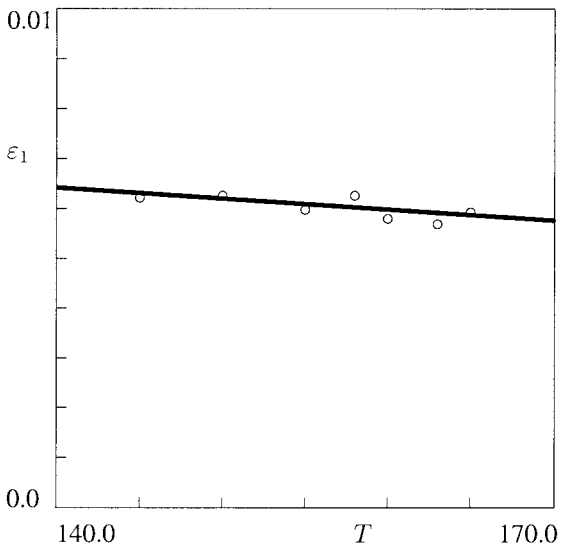

Figure 9 Strain ε_1 which characterizes a decrease in the elastic modulus at retraction versus the annealing temperature T (°C). (Circles) Treatment of observations. (Solid lines) Approximation of the experimental data by eq. (27) with $d_0 = 9.48 \times 10^{-3}$ and $d_1 = 2.19 \times 10^{-5}$.

different material parameters, γ_k, in the sub-T_c and post-T_c regions.

The strains, ε_1 and ε_2, are depicted in Figures 9 and 10. The observations are matched by the phenomenological relations

$$\varepsilon_1 = d_0 - d_1 T, \qquad \log \varepsilon_2 = g_1 + g_2 T \qquad (27)$$

where log = $\log_{10}$ and the coefficients d_k and g_k ($k = 0$, 1) are determined by the least-squares method. Figure 9 demonstrates that eqs. (27) ensure a good approximation of the experimental data for ε_1. According to Figure 10, the observations for ε_2 are correctly described by eqs. (27) with different coefficients below and above some temperature T_0 which is less than T_c by several K.

DISCUSSION

Figures 5 and 9 show that the elastic modulus, E_0, monotonically increases with the annealing temperature and the strain, ε_1, which characterizes changes in the modulus, E, caused by fragmentation of lamellar blocks, monotonically decreases with T. No pronounced effect is observed of the $\alpha_2 \rightarrow \alpha_2'$ transformation on these quantities.

The growth of E_0 with the annealing temperature, T, may be explained by lamellar thickening and secondary crystallization of the smectic mesophase, which results in an increase in the degree of crystallinity of the specimens.

According to eq. (6), a decrease in ε_1 with T means that the rate of separation of mesoregions from the ensemble at retraction grows with the annealing temperature. This conclusion appears to be quite natural, because thermal treatment of iPP causes (i) growth (thickening) of dominant lamellae, (ii) formation of thin (secondary) lamellae, and (iii) a pronounced decrease in the concentration of transverse lamellae. It is conventionally accepted[31] that the rates of these processes are inversely proportional to the degree of supercooling (the difference between the melting temperature and the temperature of annealing), which means that, given a duration of annealing, these morphological transformations in iPP become more pronounced with an increase in T.

According to ref. 31, the growth of stacked dominant lamellae results in an increase in their long period, which means that fragmentation of lamellae (modeled as ribbons twisted and bent due to deformation of surrounding amorphous regions[10]) occurs at smaller stresses. Formation of thin (secondary) lamellae does not increase significantly the rigidity of spherulites, whereas disappearance of transverse lamellae implies a pronounced reduction in the rigidity of spherulites. All these factors enhance disintegration of lamellar blocks and formation of their stacks that screen the macrostrain in occluded MRs. It follows from eqs. (6) and (18) that the latter conclusion means that the higher the annealing temperature is the smaller is the strain, ε_1, which characterizes formation of occluded mesodomains separated from the ensemble of MRs.

Figure 6 and 7 show a pronounced effect of the $\alpha_2 \rightarrow \alpha_2'$ transformation on the quantities a and ε, which

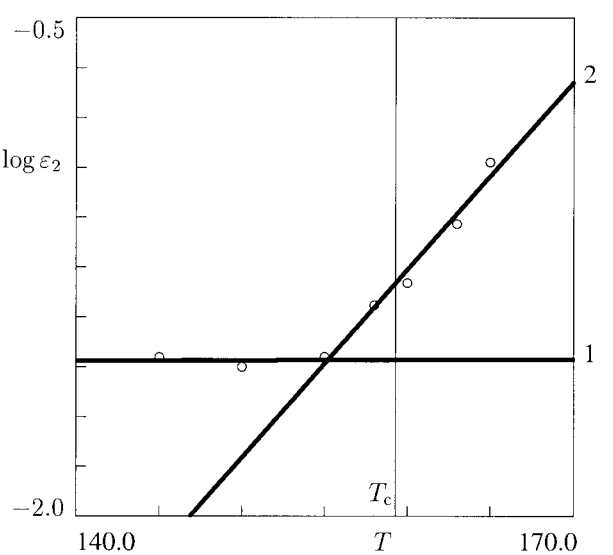

Figure 10 Strain ε_2 which characterizes changes in the rate of plastic strain ϵ_{p2} at retraction versus the annealing temperature T (°C). (Circles) Treatment of observations. (Solid lines): Approximation of the experimental data by eq. (27). (Curve 1) $g_0 = -1.55$; $g_1 = 1.31 \times 10^{-4}$; (curve 2) $g_0 = -10.29$; $g_1 = 5.64 \times 10^{-2}$.

characterize a steady plastic flow at active loading. According to Figure 6, in the sub-T_c domain, the rate, a, of a developed plastic flow weakly grows with the annealing temperature. At the critical temperature, T_c, the coefficient a experiences a jump to its maximal value, $a_{\max} = 1$. In the post-T_c domain, a strongly decreases with T and returns to the $a(T)$ curve (extrapolated from the sub-T_c region) in the close vicinity of the melting temperature, T_m. Figure 7 demonstrates a similar dependence of the strain, ε, on the temperature, T. The only difference is that ε weakly decreases with the annealing temperature below the critical temperature, T_c.

The increase in a and the decrease in ε with T in the sub-T_c domain mean that the plastic strain, ϵ_{p1}, grows with the annealing temperature. This conclusion seems quite natural, because an increase in the plastic strain, ε_{p1}, is attributed to (i) a fine slip of the lamellar blocks[18] and (ii) slippage and separation of tie chains from the lamellae.[16,17] Secondary crystallization of the smectic mesophase at annealing implies an increase in the free volume per chain in the amorphous phase (due to the difference in densities of the crystalline and amorphous phases). The latter enhances the molecular mobility inside amorphous regions (which is reflected by the model as the growth of the rate of the sliding of junctions) as well as on their boundaries (which is associated with slip of the tie chains along the lamellae).

A pronounced increase in a at the critical temperature, T_c, may be explained by a new mechanism for plastic flow driven by sliding of blocks in the α_2' lamellae. This assertion is in agreement with experimental data by Gu et al.,[8] who reported a noticeable increase in the lattice constants of the α crystallites at T_c. The growth of average sizes of unit cells implies that "molecular chains become much more mobile."[8] In the present model, the enhanced mobility of chains is reflected by an increase in the rate of a developed plastic flow. The transition from the plasticity mechanism based on the sliding of tie chains along and their separation from the lamellae to the plasticity mechanism grounded on fine slip of α_2' lamellar blocks is confirmed by a positive jump of ε at the critical temperature. The latter is associated with a pronounced increase in stresses governing the elastoplastic response (the slippage of tie chains along the lamellae occurs at substantially smaller stresses than those necessary for the fine slip of lamellar blocks).

A decrease in a and ε in the post-T_c domain shows that the α_2' crystalline phase is stable in a rather narrow interval of temperatures. Curves 2 in Figures 6 and 7 indicate that thermal treatment of specimens in the close vicinity of the melting temperature, T_m, is not favorable for the formation of the new phase: The values of a and ε return to those predicted by extrapolation of the $a(T)$ and $\varepsilon(T)$ curves from the sub-T_c domains.

Figure 8 reveals that the parameter γ decreases with the annealing temperature below the critical temperature, T_c, experiences a negative jump at T_c, and increases with T in the post-T_c domain. According to eq. (25), the same behavior is demonstrated by the rate of plastic flow, Γ_0, which characterizes the coarse slip and fragmentation of lamellar blocks. The results depicted in Figure 8 appear to be natural. A decrease in Γ_0 with the annealing temperature in the subcritical region is attributed to the growth of perfectness of lamellae at the thermal treatment (the $\alpha_1 \rightarrow \alpha_2$ transformation). The negative jump of the rate of plastic flow, Γ_0, at the critical temperature, T_c, means that the $\alpha_2 \rightarrow \alpha_2'$ transition results in formation of stronger crystallites (the new crystalline phase is less fragile due to an increase in chain mobility). Finally, an increase in Γ_0 with T above the critical temperature is associated with the fact that the new phase disappears with the growth of the annealing temperature in the close vicinity of the melting temperature.

Figure 10 shows that the parameter ε_2 is independent of the annealing temperature at thermal treatment below some threshold temperature T_0, and it monotonically grows with T above T_0. The $\alpha_2 \rightarrow \alpha_2'$ transformation does not affect the dependence $\varepsilon_2(T)$. As the increase in ε_2 with the annealing temperature begins near the temperature at which transverse lamellae disappear, we attribute the monotonous growth of the function $\varepsilon_2(T)$ to a decrease in the mechanical stability of spherulites driven by alteration of their morphology. It is worth noting that this explanation is not unambiguous, because the growth of ε_2 with T (which reflects the effect of macrostrains on a coarse slip of lamellar blocks) may be associated with the mechanisms for changes in the microstructure of individual lamellae proposed in refs. 3 and 31.

CONCLUSIONS

A series of tensile loading–unloading tests was performed on injection-molded iPP at room temperature. Experiments were carried out on a specimen not subjected to thermal treatment as well as on samples annealed for 24 h at the temperatures T = 145, 150, 155, 158, 160, 163, and 165°C, which cover the entire region of high-temperature annealing temperatures.

Constitutive equations were derived for the elastoplastic response of a semicrystalline polymer. A polymer is treated as an equivalent heterogeneous network of chains bridged by permanent junctions. The network is modeled as an ensemble of mesoregions linked with each other. At active loading in the subyield region of deformations, junctions between chains in MRs slide with respect to their reference positions (which reflects the sliding of the tie chains

and the fine slip of lamellar blocks). At retraction, this nonaffine deformation of the network is accompanied by displacements of mesodomains with respect to each other (which describe the coarse slip and fragmentation of lamellar blocks). Disintegration of lamellar blocks results in separation of some MRs from the ensemble (which reflects screening of the macrostrain in these mesodomains by surrounding lamellar stacks and the formation of occluded regions).

New kinetic equations were proposed for the evolution of plastic strains and for the rate of separation of MRs from the ensemble. Stress–strain relations for isothermal uniaxial deformation were developed by using the laws of thermodynamics. The constitutive equations are determined by six adjustable parameters that are found by fitting the experimental data. Fair agreement is demonstrated between the stress–strain curves in cyclic tests and the results of numerical simulation.

The following conclusions were drawn:

1. The elastic modulus, E_0, monotonically increases with the annealing temperature, T, due to the growth of the degree of crystallinity. The strain, ε_1, which characterizes changes in the elastic modulus at retraction, monotonically decreases with T, due to the growth of brittleness of spherulites. The $\alpha_2 \rightarrow \alpha_2'$ transformation does not affect these parameters.
2. Both rates of plastic flow, a and Γ_0, are strongly affected by the $\alpha_2 \rightarrow \alpha_2'$ phase transition. The parameter a experiences a positive jump, whereas Γ_0 demonstrates a negative jump. These changes are associated with an increased mobility of chains in α_2' crystallites that enhances the sliding of junctions, on the one hand, and leads to a decrease in the rate of lamellar fragmentation, on the other.
3. The strain, ε, which characterizes the transition to a developed plastic flow at active loading, experiences a positive jump at the critical temperature, T_c. This jump is attributed to the transition from the plastic flow associated with the sliding of tie chains along the lamellae to the flow, which reflects the fine slip of lamellar blocks in α_2' crystals.
4. The strain, ε_2, which describes the effect of the macrostrain on plastic deformation at retraction, changes continuously with the annealing temperature, T. It remains independent of T below some threshold temperature, T_0, and exponentially increases with T above T_0. The effect of the annealing temperature on ε_2 is associated with morphological transformations in spherulites that decrease their mechanical stability (in particular, with disappearance of transverse lamellae at high-temperature annealing).

References

1. Al-Raheil, I. A.; Qudah, A. M.; Al-Share, M. J Appl Polym Sci 1998, 67, 1267.
2. Yamada, K.; Matsumoto, S.; Tagashira, K.; Hikosaka, M. Polymer 1998, 39, 5327.
3. Xu, J.; Srinivas, S.; Marand, H.; Agarwal, P. Macromolecules 1998, 31, 8230.
4. Alamo, R. G.; Brown, G. M.; Mandelkern, L.; Lehtinen, A.; Paukkeri, R. Polymer 1999, 40, 3933.
5. Iijima, M.; Strobl, G. Macromolecules 2000, 33, 5204.
6. Maiti, P.; Hikosaka, M.; Yamada, K.; Toda, A.; Gu, F. Macromolecules 2000, 33, 9069.
7. Dudic, D.; Kostoski, D.; Djukovic, V.; Dramacanin, M. D. Polym Int 2001, 51, 111.
8. Gu, F.; Hikosaka, M.; Toda, A.; Ghosh, S. K.; Yamazaki, S.; Araki, M.; Yamada, K. Polymer 2002, 43, 1473.
9. Kalay, G.; Bevis, M. J. J Polym Sci B Polym Phys 1997, 35, 241, 265.
10. Coulon, G.; Castelein, G.; G'Sell, C. Polymer 1998, 40, 95.
11. Auriemma, F.; Ruiz de Ballesteros, O.; De Rosa, C.; Corradini, P. Macromolecules 2000, 33, 8764.
12. Hikosaka, M.; Seto, T. Polym J 1973, 5, 111.
13. Radhakrishnan, J.; Ichikawa, K.; Yamada, K.; Toda, A.; Hikosaka, M. Polymer 1998, 39, 2995.
14. Verma, R.; Marand, H.; Hsiao, B. Macromolecules 1996, 29, 7767.
15. Seguela, R.; Staniek, E.; Escaig, B.; Fillon, B. J Appl Polym Sci 1999, 71, 1873.
16. Nitta, K.-H.; Takayanagi, M. J Polym Sci B Polym Phys 1999, 37, 357.
17. Nitta, K.-H.; Takayanagi, M. J Polym Sci B Polym Phys 2000, 38, 1037.
18. Aboulfaraj, M.; G'Sell, C.; Ulrich, B.; Dahoun, A. Polymer 1995, 36, 731.
19. Bergström, J. S.; Kurtz, S. M.; Rimnac, C. M.; Edidin, A. A. Biomaterials 2002, 23, 2329.
20. Meyer, R. W.; Pruitt, L. A. Polymer 2001, 42, 5293.
21. Sweeney, J.; Collins, T. L. D.; Coates, P. D.; Ward, I. M. Polymer 1997, 38, 5991.
22. Sweeney, J.; Collins, T. L. D.; Coates, P. D.; Duckett, R. A. J Appl Polym Sci 1999, 72, 563.
23. Ogden, R. W.; Roxburgh, D. G. Proc R Soc Lond A 1999, 455, 2861.
24. Inberg, J. P. F.; Takens, A.; Gaymans, R. J. Polymer 2002, 43, 2795.
25. Witten, T. A.; Rubinstein, M.; Colby, R. H. J Phys II Fr 1993, 3, 367.
26. Boyce, M. C.; Parks, D. M.; Argon, A. S. Mech Mater 1988, 7, 15.
27. Hasan, O. A.; Boyce, M. C. Polym Eng Sci 1995, 35, 331.
28. Bordonaro, C. M.; Krempl, E. Polym Eng Sci 1995, 35, 310.
29. Quinson, R.; Perez, J.; Rink, M.; Pavan, A. J Mater Sci 1997, 32, 1371.
30. Spathis, G.; Kontou, E. Polymer 1998, 39, 135.
31. Hikosaka, M.; Amano, K.; Rastorgi, S.; Keller, A. Macromolecules 1997, 30, 2067.